

Qualitative Analysis and Plasma Characteristics of Soil from a Desert Area using LIBS Technique

W Aslam Farooq^{1*}, Walid Tawfik^{1,2†}, Fahad N. AL-Mutairi¹, and Zeyad A. Alahmed¹

¹Department of Physics and Astronomy, College of Science King Saud University, Riyadh, Saudi Arabia

²Department of Environmental Applications, NILES National Institute of Laser, Cairo University, Cairo, Egypt

(Received June 26, 2013 : revised October 16, 2013 : accepted October 31, 2013)

In this work, laser induced breakdown spectroscopy (LIBS) is used to investigate soil samples collected from different desert areas of Riyadh city in Saudi Arabia. Both qualitative analysis and plasma parameters are studied via the observed LIBS spectra. These experiments have been done using a Spectrolaser-7000 system with 50 mJ fundamental wavelength of Nd:YAG laser and detection delay time of 1 microsecond. Many spectral lines are highly resolved for many elements like Al, Fe, Mg, Si, Mn, Na, Ca and K. The electron temperatures Te and electron densities Ne, for the constituent of generated LIBS plasma, are determined for all the collected samples. It is found that both Te and Ne vary from one desert area to other. This variation is due to the change of the elemental concentration in different desert areas that affects the sample's matrices. Time dependent measurements have also been performed on the soil samples. While the signal-to-base ratio (SBR) reached its optimal value at 1 microsecond, the plasma parameters Ne and Te reach values of $4 \times 10^{17} \text{ cm}^{-3}$ and 9235 K, respectively, at 2.5 microsecond. The later indicate that the plasma cooling processes are slow in comparison to the previously observed results for metallic samples. The observed results show also that in the future it is possible to enhance the exploitation of LIBS in the remote on-line environmental monitoring application, by following up only the values of Ne and Te for one element of the soil desert sample using an optical fiber probe.

Keywords : Soil, LIBS, Plasma temperature, Electron density

OCIS codes : (300.6365) Spectroscopy, laser induced breakdown; (280.5395) Plasma diagnostics;
(070.4790) Spectrum analysis

I. INTRODUCTION

Laser-induced breakdown spectroscopy (LIBS) is an atomic emission spectroscopy that uses a highly energetic fast laser pulse focused on the sample to form plasma, the ablated material breaks down into atomic species and excited ionic species. LIBS can analyze any matter regardless of its physical state, be it gas, liquid or solid. LIBS has gained great interest for qualitative and quantitative analysis for many materials including, nano-ceramics, polymers semiconductors etc, because of its ease of use, fast response and high sensitivity [1-4]. Furthermore, remote analysis of the full elemental composition of a sample is achieved via properly optimized LIBS technique [3]. By means of *in-situ* analysis, both the complexity and the cross contamination of the detection process could be

minimized [5]. LIBS is a quite straightforward plasma spectroscopy technology, using high intensity laser pulses ($\sim 1 \text{ TW/cm}^2$) focused on a sample, thus producing plasma and ablating a very small amount of material. The produced plasma expands then cools with time, and the characteristic atomic emission lines of the elemental content in the sample could be observed. The spectral lines' intensities for particular elements are proportional to the elements' concentration in the sample. In recent years, the growing technique of LIBS has been applied broadly with increasing success in the qualitative and quantitative analyses of soil components and additives with relevant simplification of the conventional methodologies [1-4]. However, the LIBS technique still needs additional verification before it can be implemented effectively in environmental soil analyses.

Corresponding authors: *wafarooq@hotmail.com, †wmohamed@ksu.edu.sa

Color versions of one or more of the figures in this paper are available online.

Soils represent a crucial constituent in the biogeochemical carbon cycle, and their abilities to store carbon are higher than those of biomass plants by several times. Hence, quantification of soil carbon in field conditions has a significant challenge corresponding to global climatic changes and the carbon cycle. Recently, Da Silva *et al.* [6] succeeded in calibrating a portable LIBS system to execute quantitative measurements of carbon content in a tropical soil sample. Even though their LIBS system was used for qualitative elemental analyses with no prior sample treatment, the results were obtained directly. The obtained results demonstrate the significant impact of implementing portable LIBS systems for both qualitative and quantitative analysis of carbon content in tropical soils. Santos Jr. *et al.* [7] aimed to validate the capability of LIBS to detect cadmium ions in soils since cadmium is considered as a high toxicity potential agent and can be accumulated in the living organisms. They established a computerized fast pre-processing series of algorithms for converting a sequence of several hundreds of LIBS spectra collected from a single target into an accurate enhanced spectrum. The observed spectrum provides a procedure to determine its spectral elements and a series of calibration-curves using multi-cation sulfates and standard hydrous. They were capable to observe the concentrations of Ca, S, Al, K, Mg, Fe, Na, H, and O in sulfates, along with the degrees of hydration of Mg-sulfates and Ca-sulfates, from LIBS spectra [7].

In the present study, we aim to use the LIBS technique to investigate soil samples that are collected from deserts in various locations around Riyadh city in Saudi Arabia. The spectra of major and trace elemental compositions of collected soil samples are studied. The time dependence of electron temperature and density for the observed plasma on the soil matrix is also investigated.

II. EXPERIMENTAL PROCEDURE

2.1. Samples

In the present work, four different soil samples were collected from four various locations from desert around Riyadh city. Sample-1 (ES) was collected from the east, 25 Km from the center of Riyadh. Sample-2 (NS) was collected from the north, 20 Km from the center of Riyadh. Sample-3 (WS) was collected from the east, 30 Km from the center of Riyadh. Sample-4 (SS) was collected from the south 50 Km from the center of Riyadh and close to Al-Kharj city. Locations of the samples are shown in the map given in Fig. 1. These samples were ground then pressed into pellets of 30 mm diameters using pressure of 20 tons for 15 minutes.

2.2. LIBS System

The schematic diagram of the LIBS experimental setup was shown elsewhere before in detail [5]. Briefly, in the current setup the LIBS experiment was carried out using a compact LIBS system spectrolaser model 7000 from Laser Analysis Technologies, Australia. The latter is a complete



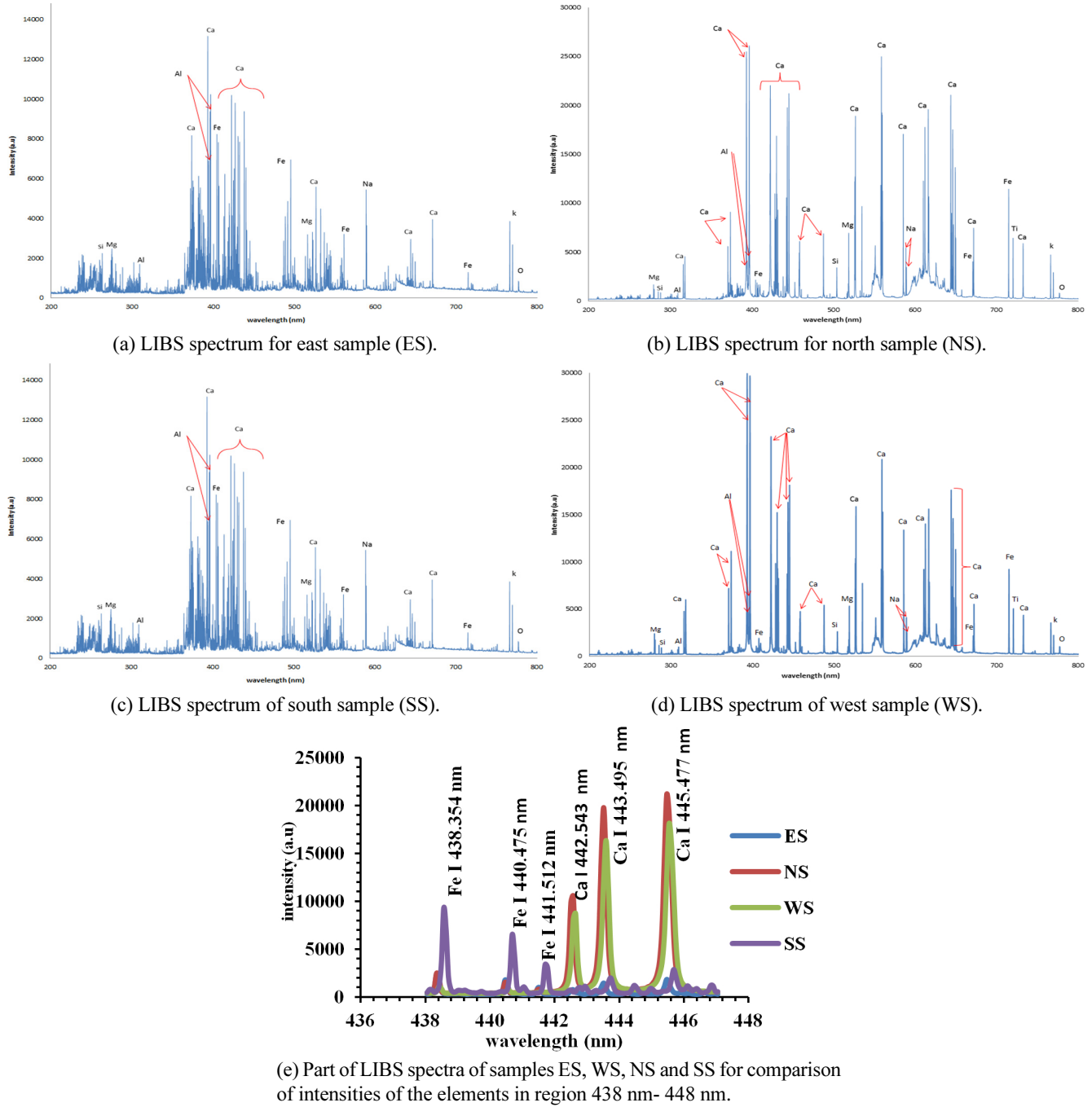
FIG. 1. Location for collected samples ES, NS, WS and SS at a desert of Riyadh city, Saudi Arabia.

integrated system containing a Nd:YAG laser as an excitation source, high resolution optical spectrograph, focusing optics, sample chamber, optical fibers, and CCD detectors with special data acquisition software. The excitation laser source is a high power Q-switched pulsed Nd:YAG of 7 ns pulse at the first harmonic 1,064 nm for energy ranges 5-300 mJ and repetition rate of 10 Hz. The system could focus on a fresh region of the sample through an x-y translation stage for the successive laser pulses. In the current study, laser energy of 50 mJ has been used with a CDD detector of a varied delay time and fixed gate width of 1 μ s (the gate width could not be changed for that system). Using a convex lens of 45 mm focal length, the laser beam was focused at the target to ablate material from the sample surface and produce a plasma plume. A bundle of optical fiber (600 μ m in diameter) was used to collect the radiation emitted by the generated plasma. This collected light was then analyzed using a high-resolution spectrometer (\sim 0.1 nm FWHM) attached to a gated CCD. To minimize the noise, an average of 10 collected spectra was recorded for each LIBS spectrum, for the full active range from 190~1,100 nm.

III. RESULTS AND DISCUSSION

3.1. LIBS Spectrum

Typical LIBS soil spectra for the spectral range from 200 nm to 800 nm are shown in Figs. 2(a)-(d), for ES, NS, SS, and WS soil samples respectively, using spectrolaser software provided with the "Spectrolaser" LIBS system. The obtained results revealed that the concentration of elemental content of the soil samples varied from one desert area to another. This is clear by comparing the relative intensities of the spectral lines for the four samples as shown in Fig. 2(e). The latter figure demonstrates the observed spectral lines' intensities for iron and calcium in the spectral region 438 nm - 448 nm include: Fe I 438.354 nm, Fe I 440.475 nm, Fe I 441.512 nm and Ca I 442.543 nm, Ca I 443.495 nm, Ca I 445.477 nm. Using a fixed laser energy value, the relative intensities for iron lines are higher for SS samples



(e) Part of LIBS spectra of samples ES, WS, NS and SS for comparison of intensities of the elements in region 438 nm- 448 nm.

FIG. 2. LIBS spectra for ES, NS, SS, and WS collected soil samples.

than for others while the relative intensities for calcium lines are high for NS, WS samples compared to other samples. Since the change of the line intensity is associated with change of the elemental concentration; the observed result revealed that the concentration of elemental content of soil varied from one area to another. A list of 106 resolved spectral lines of the elements along with all spectroscopic data for the investigated samples is given in Table 1.

3.2. Characterization of Laser Induced Plasma

3.2.1. Plasma Temperature

The ablated mass of the sample depends on the physical properties of the sample, the absorption of the incident laser beam radiation by the surface, the plasma-shielding, which is associated with the electron density of the plasma, and the laser flounce [14-15]. Hence, studying the plasma temperature and the density of plasma species is essential for the understanding of the dynamics of ionization, the dissociation-

TABLE 1. The spectroscopic data for the resolved spectral lines of soil samples for the range from 200 nm-800 nm (continued)

Element wavelength (nm)	A_{ki} (S^{-1})	E_i (cm^{-1})	E_k (cm^{-1})	Configurations	g_k
Fe II 234.83	1.15E+08	667.683	43 238.586	$3d^6(^5D)4s - 3d^6(^5D)4p$	6
Fe II 235.99	3.59E+07	1 872.567	44 232.512	$3p^63d^7 - 3d^6(^5D)4p$	10
Fe II 238.203	3.13E+08	0	41 968.046	$3d^6(^5D)4s - 3d^6(^5D)4p$	12
Fe II 239.542	2.67E+07	667.683	42 401.302	$3d^6(^5D)4s - 3d^6(^5D)4p$	4
Fe II 240.488	1.96E+08	667.683	42 237.033	$3d^6(^5D)4s - 3d^6(^5D)4p$	8
Fe II 241.052	1.55E+08	862.613	42 334.822	$3d^6(^5D)4s - 3d^6(^5D)4p$	6
Fe I 252.429	3.23E+08	888.132	40 491.284	$3d^64s^2 - 3d^6(^5D)4s4p(^1P^\circ)$	1
Fe II 256.253	1.79E+08	7 955.299	46 967.444	$3d^6(^5D)4s - 3d^6(^5D)4p$	6
Fe II 259.836	1.43E+08	384.79	38 858.958	$3d^6(^5D)4s - 3d^6(^5D)4p$	6
Fe II 273.954	2.21E+08	7 955.299	44 446.878	$3d^6(^5D)4s - 3d^6(^5D)4p$	8
Fe II 274.319	1.97E+08	8 846.768	45 289.801	$3d^6(^5D)4s - 3d^6(^5D)4p$	4
Fe II 274.648	2.05E+08	8 680.454	45 079.879	$3d^6(^5D)4s - 3d^6(^5D)4p$	6
Fe II 274.698	1.69E+08	8 391.938	44 784.761	$3d^6(^5D)4s - 3d^6(^5D)4p$	13
Fe II 275.329	1.89E+08	26 352.766	62 662.244	$3d^6(^3H)4s - 3d^6(^3H)4p$	12
Fe II 275.573	2.15E+08	7 955.299	44 232.512	$3d^6(^5D)4s - 3d^6(^5D)4p$	10
Fe I 292.911	1.53E+08	26 627.609	60 757.596	$3d^7(^2H)4s-3d^6(^3H)4s4p(^1P^\circ)$	9
Fe I 293.69	1.40E+07	0	34 039.516	$3d^64s^2 - 3d^7(^4F)4p$	9
Fe I 294.787	1.83E+07	415.933	34 328.752	$3d^64s^2 - 3d^7(^4F)4p$	7
Fe I 296.689	2.72E+07	0	33 695.397	$3d^64s^2 - 3d^7(^4F)4p$	11
Fe I 297.323	1.83E+07	415.933	34 039.516	$3d^64s^2 - 3d^7(^4F)4p$	9
Fe II 298.482	4.29E+07	13 474.411	46 967.444	$3p^63d^7 - 3d^6(^5D)4p$	6
Fe I 299.442	4.39E+07	415.933	33 801.572	$3d^64s^2 - 3d^7(^4F)4p$	5
Fe I 302.063	7.59E+07	0	33 095.941	$3d^64s^2 - 3d^7(^4F)4p$	9
Fe I 303.738	2.91E+07	888.132	33 801.572	$3d^64s^2 - 3d^7(^4F)4p$	5
Fe I 305.744	3.13E+07	6 928.268	39 625.804	$3d^7(^4F)4s - 3d^6(^5D)4s4p(^1P^\circ)$	9
Fe I 338.397	6.52E+06	17 550.181	47 092.712	$3d^7(^4P)4s - 3d^6(^3F^2)4s4p(^3P^\circ)$	7
Fe I 344.236	4.55E+06	18 378.186	47 419.687	$3d^64s^2 - 3d^6(^3P^2)4s4p(^3P^\circ)$	5
Fe I 357.2	2.89E+07	22 845.869	50 833.438	$3d^6(^5D)4s4p(^3P^\circ) - 3d^6(^5D)4s(^6D)4d$	11
Fe I 368.6	3.34E+07	23 711.456	50 833.438	$3d^6(^5D)4s4p(^3P^\circ) - 3d^6(^5D)4s(^6D)4d$	11
Fe I 373.532	2.70E+07	23 711.456	50 475.288	$3d^6(^5D)4s4p(^3P^\circ) - 3d^6(^5D)4s(^6D)4d$	9
Fe I 404.581	8.62E+07	11 976.239	36 686.176	$3d^7(^4F)4s - 3d^7(^4F)4p$	9
Fe I 406.359	6.65E+07	12 560.934	37 162.746	$3d^7(^4F)4s - 3d^7(^4F)4p$	7
Fe I 420.203	8.22E+07	11 976.239	35 767.564	$3d^7(^4F)4s - 3d^7(^4F)4p$	9
Fe I 421.034	1.48E+07	20 019.635	43 763.980	$3d^6(^5D)4s4p(^3P^\circ) - 3d^6(^5D)4s(^6D)5s$	3
Fe I 425.079	1.02E+07	12 560.934	36 079.372	$3d^7(^4F)4s - 3d^7(^4F)4p$	7
Fe I 426.047	3.99E+07	19 350.891	42 815.855	$3d^6(^5D)4s4p(^3P^\circ) - 3d^6(^5D)4s(^6D)5s$	11
Fe I 427.175	2.28E+07	11 976.239	35 379.208	$3d^7(^4F)4s - 3d^7(^4F)4p$	11
Fe I 430.79	3.38E+07	12 560.934	35 767.564	$3d^7(^4F)4s - 3d^7(^4F)4p$	9
Fe I 432.576	5.16E+07	12 968.554	36 079.372	$3d^7(^4F)4s - 3d^7(^4F)4p$	7
Fe I 438.354	5.00E+07	11 976.239	34 782.421	$3d^7(^4F)4s - 3d^7(^4F)4p$	11
Fe I 440.475	2.75E+07	12 560.934	35 257.324	$3d^7(^4F)4s - 3d^7(^4F)4p$	9
Fe I 441.512	1.19E+07	12 968.554	35 611.625	$3d^7(^4F)4s - 3d^7(^4F)4p$	7

TABLE 1. The spectroscopic data for the resolved spectral lines of soil samples for the range from 200 nm-800 nm (continued)

Element wavelength (nm)	A_{ki} (S^{-1})	E_i (cm^{-1})	E_k (cm^{-1})	Configurations	g_k
Fe II 453.416	2.30E+07	23 031.300	45 079.879	$3d^6(^3F^2)4s - 3d^6(^5D)4p$	6
Fe I 455.445	4.70E+07	23 110.939	45 061.329	$3d^6(^5D)4s4p(^3P^o) - 3d^6(^5D)4s(^6D)5s$	7
Fe I 492.05	3.58E+07	22 845.869	22 845.869	$3d^6(^5D)4s4p(^3P^o) - 3d^6(^5D)4s(^6D)5s$	9
Fe I 495.76	4.22E+07	22 650.416	42 815.855	$3d^6(^5D)4s4p(^3P^o) - 3d^6(^5D)4s(^6D)5s$	11
Fe I 520.859	6.23E+06	26 140.179	45 333.875	$3d^6(^5D)4s4p(^3P^o) - 3d^6(^5D)4s(^6D)5s$	5
Fe I 526.953	1.27E+06	6 928.268	25 899.989	$3d^7(^4F)4s - 3d^6(^5D)4s4p(^3P^o)$	9
Fe I 532.804	1.15E+07	7 376.764	26 140.179	$3d^7(^4F)4s - 3d^6(^5D)4s4p(^3P^o)$	7
Fe I 537.149	1.05E+07	7 728.060	26 339.696	$3d^7(^4F)4s - 3d^6(^5D)4s4p(^3P^o)$	5
Fe I 540.577	1.09E+07	7 985.785	26 479.381	$3d^7(^4F)4s - 3d^6(^5D)4s4p(^3P^o)$	3
Fe I 558.676	2.19E+07	27 166.820	45 061.329	$3d^6(^5D)4s4p(^3P^o) - 3d^6(^5D)4s(^6D)5s$	7
Fe I 616.536	6.54E+05	33 412.717	49 627.884	$3d^8 - 3d^7(^2G)4p$	9
Si I 243.515	4.43E+07	6 298.850	47 351.554	$3s^23p^2 - 3s^23p3d$	5
Si I 250.689	5.47E+07	77.115	39 955.053	$3s^23p^2 - 3s^23p4s$	5
Si I 251.431	7.39E+07	0	39 760.285	$3s^23p^2 - 3s^23p4s$	3
Si I 251.611	1.68E+08	223.157	39 955.053	$3s^23p^2 - 3s^23p4s$	5
Si I 263.128	1.06E+08	15 394.370	53 387.334	$3s^23p^2 - 3s^23p3d$	3
Si I 288.157	2.17E+08	6 298.850	40 991.884	$3s^23p^2 - 3s^23p4s$	3
Si I 390.552	1.33E+07	15 394.370	40 991.884	$3s^23p^2 - 3s^23p4s$	3
Al I 237.312	8.60E+07	112.061	42 237.783	$3s^23p - 3s^24d$	6
Al I 308.215	6.30E+07	0	32 435.453	$3s^23p - 3s^23d$	4
Al I 309.27	7.40E+07	112.061	32 436.796	$3s^23p - 3s^23d$	6
Al I 394.4	4.93E+07	0	25 347.756	$3s^23p - 3s^24s$	2
Al I 396.152	9.80E+07	112.061	25 347.756	$3s^23p - 3s^24s$	2
Mg II 279.07	4.01E+08	35 669.31	71 491.06	$2p^63p - 2p^63d$	4
Mg II 279.552	2.60E+08	0	35 760.88	$2p^63s - 2p^63p$	4
Mg II 279.79	7.98E+07	35 760.88	71 491.06	$2p^63p - 2p^63d$	4
Mg II 280.27	2.57E+08	0	35 669.31	$2p^63s - 2p^63p$	2
Mg I 285.212	4.91E+08	0	35 051.264	$2p^63s^2 - 3s3p$	3
Mg I 383.829	1.61E+08	21 911.178	47 957.045	$3s3p - 3s3d$	7
Mg I 516.732	1.13E+07	21 850.405	41 197.403	$3s3p - 3s4s$	3
Mg I 517.268	3.37E+07	21 870.464	41 197.403	$3s3p - 3s4s$	3
Mg I 518.36	5.61E+07	21 911.178	41 197.403	$3s3p - 3s4s$	3
Ca II 315.88	3.10E+08	25 191.51	56 839.25	$3p^64p - 3p^64d$	4
Ca II 317.933	3.60E+08	25 414.40	56 858.46	$3p^64p - 3p^64d$	6
Ca II 393.366	1.47E+08	0	25 414.40	$3p^64s - 3p^64p$	4
Ca II 396.847	1.40E+08	0	25 191.51	$3p^64s - 3p^64p$	2
Ca 422.673	2.18E+08	0	23 652.304	$3p^64s^2 - 3p^64s4p$	3
Ca I 428.301	4.34E+08	15 210.063	38 551.558	$3p^64s4p - 3p^64p^2$	5
Ca I 428.936	6.00E+07	15 157.901	38 464.808	$3p^64s4p - 3p^64p^2$	3
Ca I 430.252	1.36E+08	15 315.943	38 551.558	$3p^64s4p - 3p^64p^2$	5
Ca I 443.495	6.70E+07	15 210.063	37 751.867	$3p^64s4p - 3p^64s4d$	5
Ca I 445.477	8.70E+07	15 315.943	37 757.449	$3p^64s4p - 3p^64s4d$	7

TABLE 1. The spectroscopic data for the resolved spectral lines of soil samples for the range from 200 nm-800 nm (continued)

Element wavelength (nm)	$A_{ki} (\text{s}^{-1})$	$E_i (\text{cm}^{-1})$	$E_k (\text{cm}^{-1})$	Configurations	g_k
Ca I 559.446	3.80E+07	20 349.260	38 219.118	$3p^63d4s - 3p^63d4p$	5
Ca I 559.848	4.30E+07	20 335.360	38 192.392	$3p^63d4s - 3p^63d4p$	3
Ca I 610.272	9.60E+06	15 157.901	31 539.495	$3p^64s4p - 3p^64s5s$	3
Ca I 612.221	2.87E+07	15 210.063	31 539.495	$3p^64s4p - 3p^64s5s$	3
Ca I 643.907	5.30E+07	20 371.000	35 896.889	$3p^63d4s - 3p^63d4p$	9
Ca I 646.256	4.70E+07	20 349.260	35 818.713	$3p^63d4s - 3p^63d4p$	7
Ca I 649.378	4.40E+07	20 335.360	35 730.454	$3p^63d4s - 3p^63d4p$	5
Na I 261.181	2.20E+08	293 220.33	331 496.51	$2s^22p^53p - 2s^22p^5(^2P_{3/2})4s$	5
Na I 413.082	5.17E+04	16973.3669	41 174.705	$2p^63p - 2p^620d$	6
Na I 414.409	4.01E+04	16973.3669	41 097.271	$2p^63p - 2p^619s$	2
Na I 568.263	1.01E+04	16956.1705	34 548.764	$2p^63p - 2p^64d$	4
Na I 568.820	1.21E+07	16973.3669	34 548.729	$2p^63p - 2p^64d$	6
Na I 588.994	6.16E+07	0	16973.366	$2p^63s - 2p^63p$	4
Na I 589.592	6.14E+07	0	16956.170	$2p^63s - 2p^63p$	2
Mn II 293.305	2.00E+08	9472.97	43557.14	$3d^5(6S)4s - 3d^5(6S)4p$	3
Mn II 293.931	1.90E+08	9472.97	43484.64	$3d^5(6S)4s - 3d^5(6S)4p$	5
Mn II 294.92	1.90E+08	9472.97	43370.51	$3d^5(6S)4s - 3d^5(6S)4p$	7
Mn I 403.079	1.70E+07	0	24802.25	$3d^54s^2 - 3d^5(6S)4s4p(^3P^{\circ})$	8
Mn I 403.306	1.58E+07	0	24779.32	$3d^54s^2 - 3d^5(6S)4s4p(^3P^{\circ})$	4
K I 766.491	3.80E+07	0	13042.896	$3p^64s - 3p^64p$	4
K I 769.897	3.75E+07	0	12985.185	$3p^64s - 3p^64p$	2

atomization, and excitation processes occurring in the plasma [9]. The population density of atomic electronic and ionic states could be expressed using the Boltzmann distribution function if the laser induced-plasma fulfills the local thermodynamic equilibrium (LTE) condition. For low-density optically thin plasma, the effects due to re-absorption of plasma emission can be neglected [2]. Consequently, the intensity of the emitted spectral line (I) can be determined from the fractional population of the corresponding energy level of a particular element in the plasma. The plasma electron temperature can be calculated via the excitation state intensity of the emitted spectral line (I) using the well-known Boltzmann equation [17], if the plasma satisfies the LTE condition as:

$$\ln \frac{I\lambda}{A_{ki} g_k} = -\frac{1}{KT} E_k + \ln \frac{C \cdot F}{U(T)} \quad (1)$$

where λ is the wavelength (cm), g_k is the statistical weight for the upper level, A_{ki} is the transition probability (s^{-1}), T is the plasma electron temperature (Kelvin), E_k is the excited level energy (cm^{-1}), $U(T)$ is the partition function, K is the Boltzmann constant, C is the species concentration and F is an experimental factor.

From the slope of the plot of the left hand side of Eq. (1) vs. the excited level energy E_k , the plasma temperature

T can be calculated. Throughout the initial steps of plasma formation, an intense continuum (Bremsstrahlung radiation) predominates in the emitted spectrum. Thus, many heavily-broadened ionic lines of the elements present are overlaid. The main physical causes of the spectral line-broadening are the Stark broadening and the Doppler broadening. Stark broadening due to collisions of charged species is taking place at this early period. Additionally, the spectral lines of the excited neutral atoms are rather weak, and they regularly coincide with the strong ionic lines. Therefore, the isolation and observation of neutral lines are difficult [5].

Thus, the continuum can be avoided by longer delay detection time. Nevertheless, each particular spectral-line reveals different temporal evolution that relates to specific atomic energy level of the corresponding element. In order to calculate Te plasma electron temperature of the soil samples, the Boltzmann plot was determined for the resolved spectral lines of the elemental contents (Ca, Fe, Al, Si and Mg). Then an average value of all temperature values of corresponding elements in each sample was determined and listed in Table 2. The Boltzmann graph was plotted between $\ln(I\lambda/gA)$ and $(E \text{ in } \text{cm}^{-1})$ according to the formula given in equation (1). The Boltzmann graphs for Fe, Ca, Al, Si and Mg elements in NS and NE samples are depicted in Figs. 3(a)-(d).

TABLE 2. The plasma electron temperature T_e using spectral lines of Fe, Mg, Si, Al and Ca for soil samples NS, WS, ES and SS

Sample No.	Electron temperature (Kelvin) using Fe lines	Electron temperature (Kelvin) using Mg lines	Electron temperature (Kelvin) using Si lines	Electron temperature (Kelvin) using Al lines	Electron temperature (Kelvin) using Ca lines	Average Electron temperature (Kelvin)
NS	8248	8363	8387	8095	8220	$8262.6 \pm 1.42\%$
WS	8127	8329	8272	8491	8552	$8354.2 \pm 1.8\%$
ES	8196	8229	8339	8281	8036	$8216.2 \pm 1.2\%$
SS	8154	8127	8145	8486	8276	$8237.6 \pm 1.6\%$

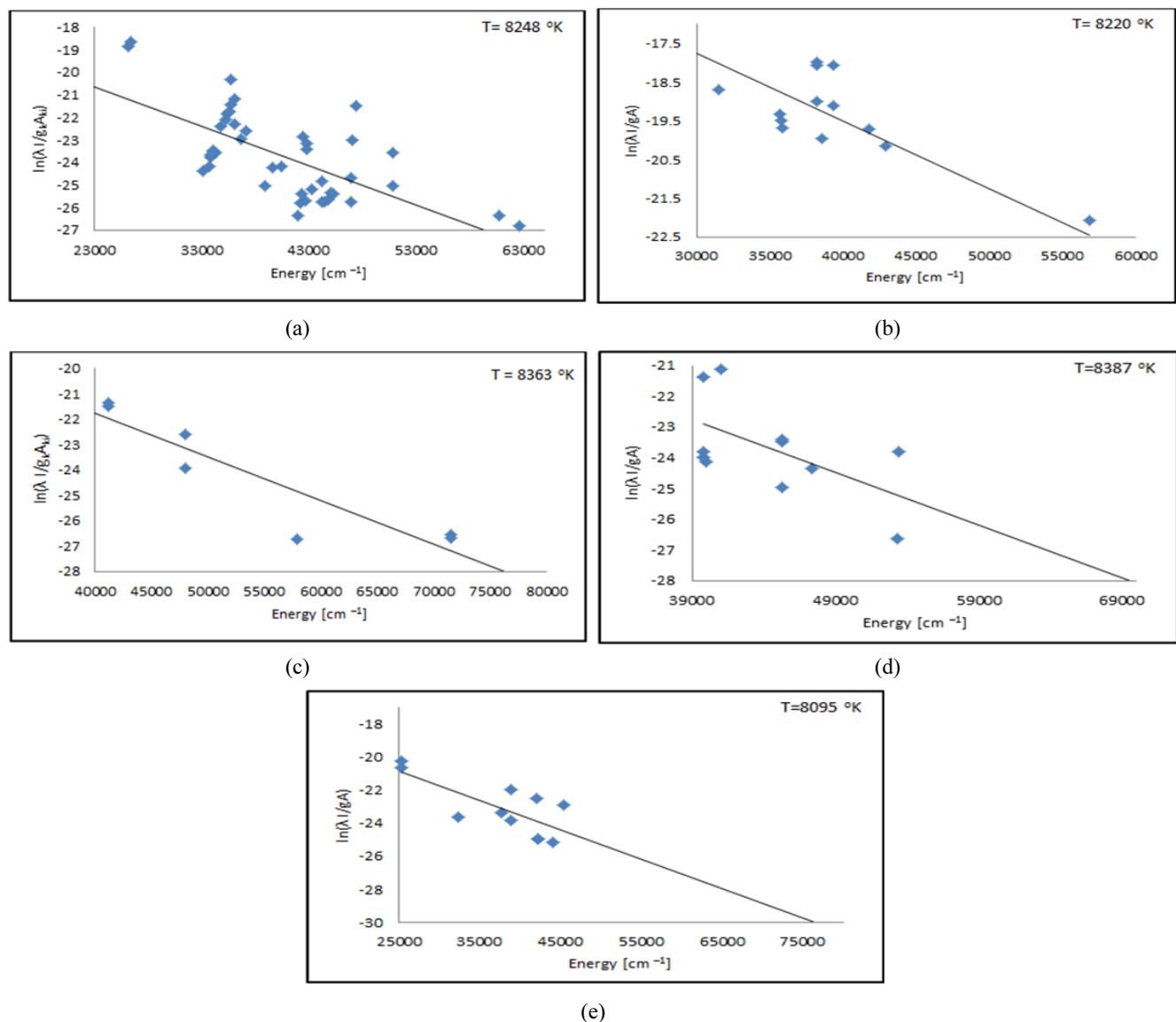


FIG. 3. The Boltzmann graphs for Fe, Ca, Al, Si and Mg elements in NS and NE samples. (a) Boltzmann plot of iron (Fe) for north soil sample (NS), (b) Boltzmann plot of calcium (Ca) for north soil sample (NS), (c) Boltzmann plot of magnesium (Mg) for north soil sample (NE), (d) Boltzmann plot of silicon (Si) for north soil sample (NE).

3.2.2. Electron Density

The plasma electron-density N_e is observed by measuring the fundamental width at half maximum FWHM ($\Delta\lambda_{1/2}$)

broadening of an appropriate emission line of the laser-plasma spectrum. The spectral width of Stark broadening for an elemental-emission line depends on the electronic density

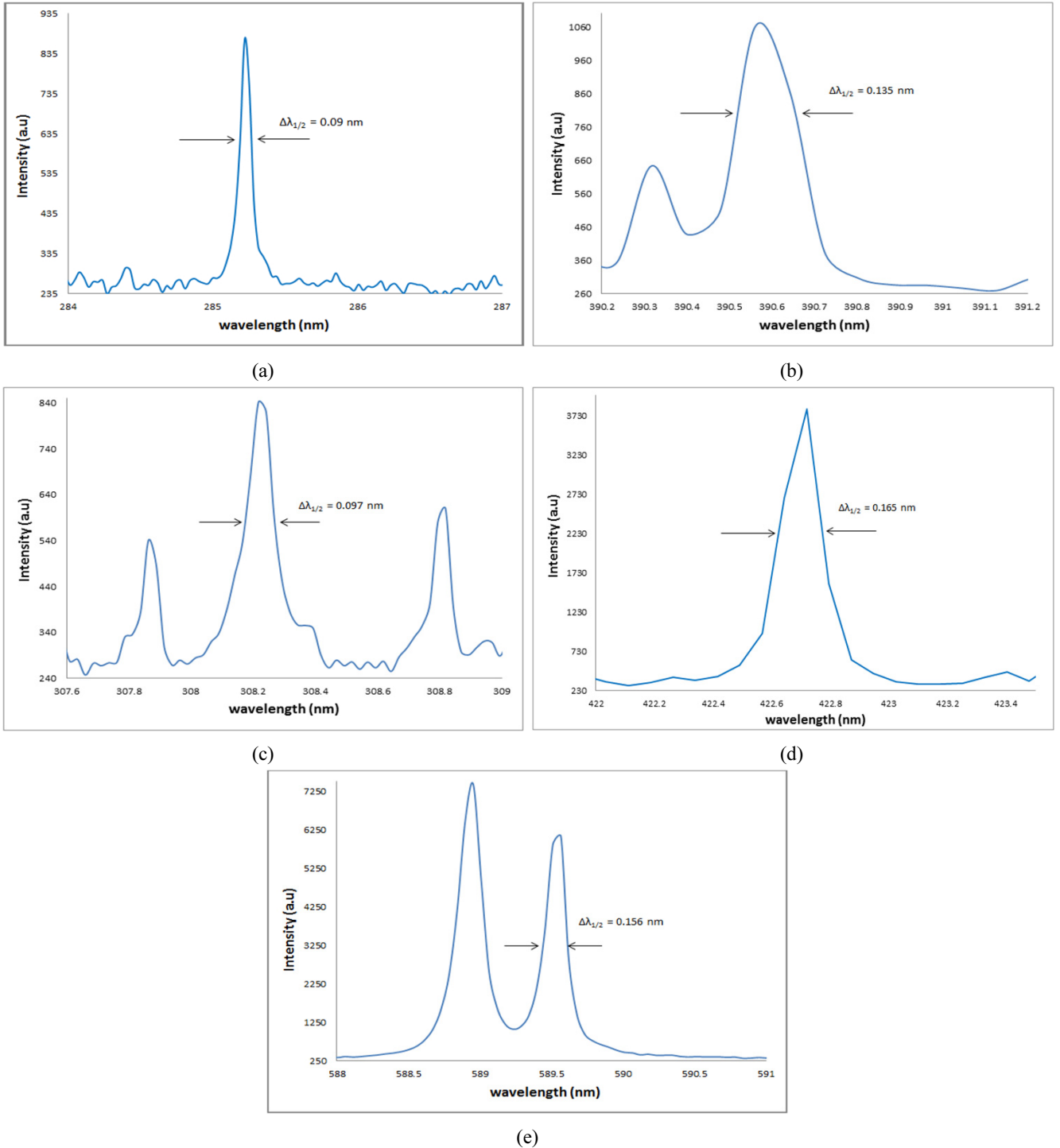


FIG. 4. Measurements of FWHM ($\Delta\lambda_{1/2}$) for Mg, Ca, Si, Al, and Na. (a) (FWHM) for Mg at 285.212 nm, (b) (FWHM) for Si at 390.552 nm, (c) (FWHM) for Al at 308.215 nm, (d) (FWHM) for Ca at 422.673 nm, (e) (FWHM) for Na at 589.592 nm.

[2]. For a non-H-like spectral line, the N_e (in cm^{-3}) is determined from the ($\Delta\lambda_{1/2}$) of the line from the following formula [9-13] ;

$$N_e \approx \left(\frac{\Delta\lambda_{FWHM}}{2.w} \right) \cdot 10^{16} \quad (2)$$

where w (nm) is the Stark broadening value or electron impact parameter [10]. This formula is commonly used for considering N_e of a plasma produced from solid targets [11]. Measurements of FWHM ($\Delta\lambda_{1/2}$) for Mg (285.212 nm), Ca (422.673 nm), Si (390.552 nm), Al (308.215 nm), and Na (589.592 nm) are shown in Figs. 4(a)-(f), respectively.

The Stark broadening values used to calculate the electronic

TABLE 3. Electron density N_e using spectral lines of Mg, Ca, Al, Na and K for soil samples NS, WS, ES and SS

Sample No.	Electron density (cm^{-3}) using Mg lines	Electron density (cm^{-3}) using Calines	Electron density (cm^{-3}) using Silines	Electron density (cm^{-3}) using Allines	Electron density (cm^{-3}) using Nalines	Electron density (cm^{-3}) using Klines	Average N_e (cm^{-3})
wavelength (nm)	285.212	422.683	390.552	308.215	589.592	766.489	-
Stark broadening (nm)	4.10E-04	6.30E-04	1.17E-03	2.60E-03	1.57E-03	4.15E-03	-
WS	9.65E+17	2.76E+18	6.41E+17	1.42E+17	4.96E+17	2.36E+17	8.73E+17
ES	9.87E+17	1.38E+18	4.35E+17	1.00E+17	3.85E+17	2.06E+17	5.82E+17
NS	9.63E+17	3.65E+18	3.97E+17	1.34E+17	3.88E+17	2.22E+17	9.59E+17
SS	1.04E+18	1.16E+18	4.74E+17	1.69E+17	4.20E+17	2.36E+17	5.83E+17

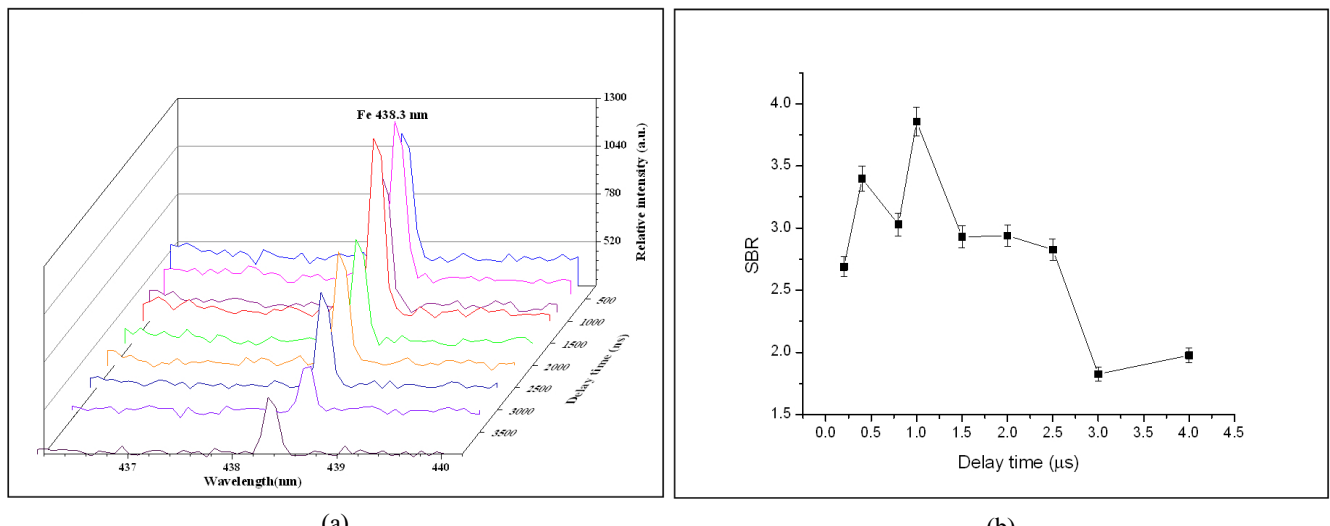


FIG. 5. (a) The variation of Fe 438.354 nm line intensity with delay time, (b) The variation of SBR for the Fe 438.354 nm with delay time.

density of detected elements in this work are given in Table 3 from Ref [10]. Electron density N_e calculated for Mg (285.212 nm), Ca (422.673 nm), Si (390.552 nm), Al (308.215 nm), and Na (589.592 nm) for all samples are given in Table 3 as well. The higher N_e values for calcium and magnesium are expected to be due to additional intensity values for resonance lines that experience self-absorption, which returns broader lines. Fig. 2. above demonstrated that the sodium concentration is very high compare to other elements that Ca and Mg. These elements are expected to be major elements represent 30-40% of the content of our collected samples. The rest of N_e values for the other elements have the same order of magnitude with error of 10-20%.

3.2.3. Time Dependent Measurements

The time resolved LIBS measurements have been applied for the soil samples using the same experimental conditions (mentioned above) under a varying delay time. Figs. 5(a), (b) demonstrates the variation of Fe 438.354 nm atomic line intensity and its signal-to-baseline ratio (SBR) with delay times from 200 ns up to 4 μ s for soil sample NS. The

figure revealed that the maximum SBR for the 438.3 nm line reached a maximum value at 1 μ s delay time. For studying the time resolved plasma characteristics of our soil sample, we have to select suitable resolved lines with the needed spectroscopic data for any of the sample elemental content as represented before in Table 2. For iron, we used the resolved ionic line Fe 239.542 nm with its Stark broadening value (1.17×10^{-2} nm) from ref. [16] to determine the plasma electron density N_e using Eq. (2).

Figure 6(a), represents the LLorentzian curve fitting of Fe 239.542 nm line to determine the variation of FWHM with delay time. The temporal behavior of the electron density, shown in Fig. 6(b), demonstrates the effect of collisional processes by the value of the electron density which increases gradually at the early time of the plasma evolution, till it reaches a maximum value, while the recombination processes are recognized at longer delay time. It is found that N_e reaches its maximum value of $4.0 \times 10^{17} \text{ cm}^{-3}$ at 2.5 μ s then cooling increased with time.

For the plasma electron temperature T_e , we used the resolved lines listed at Table 1 to determine the Boltzmann

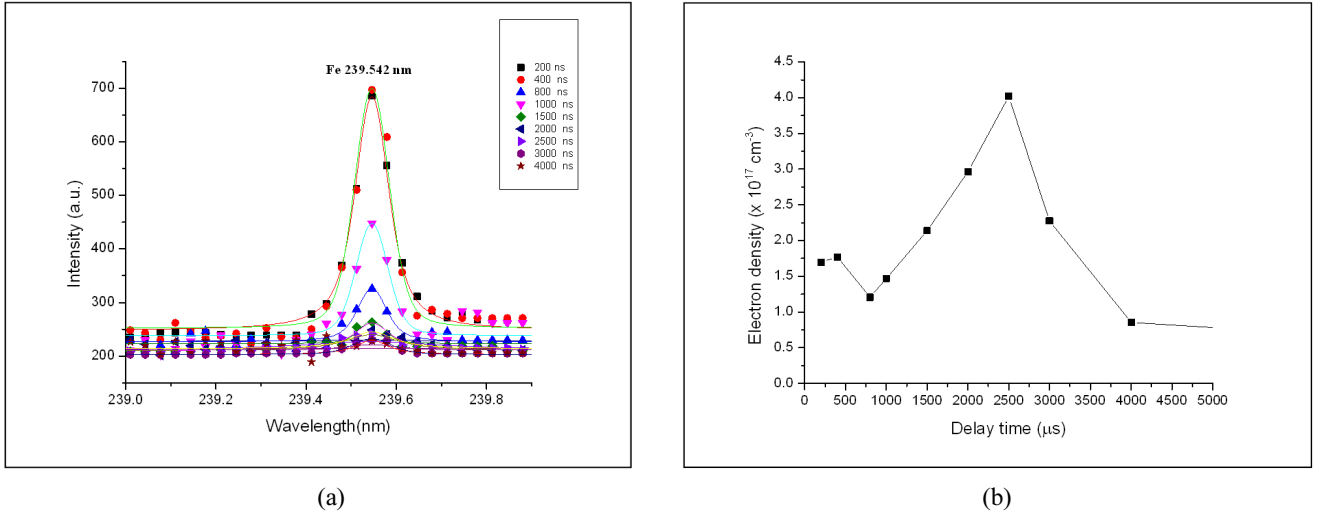


FIG. 6. (a) The Lorentzian curve fitting of Fe 239.542 nm line to determine the variation of FWHM with delay time, (b) The variation of the plasma electron density with delay time.

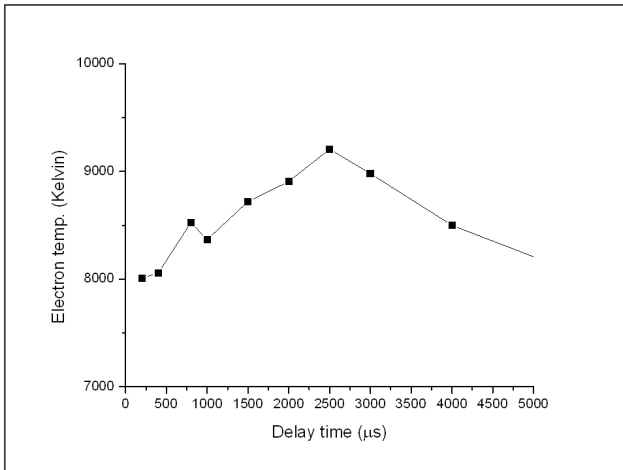


FIG. 7. The variation of the plasma electron temperature of the Fe in soil sample with delay time.

plot as represented before in Fig. 3(a) using Boltzmann Eq. (1). Fig. 7. demonstrates the variation of the plasma electron temperature of the Fe with delay time. The later figure revealed that T_e has a temporal profile similar to N_e , i.e. T_e increases with the delay time and reaches its maximum value of 9,235 K at 2.5 μs then cooling increased with time. This performance of plasma is different from metallic materials which have much faster recombination processes at early times followed by slow dynamics at longer ones as founded by our group before [11].

Finally, by considering the plasma temperature and the electron density we can examine the validity of the local thermodynamic equilibrium (LTE) assumption by considering the criterion given by McWhirter [17].

The lower limit condition for electron density at which the plasma can be considered in LTE is:

$$N_e \geq 1.4 \times 10^{12} x \Delta E^3 x T^{1/2} \quad (3)$$

T is the plasma temperature, and ΔE is the largest transitional energy for which the condition lasts [18].

In the present study $\Delta E = 5.278$ eV for Fe (as listed in Table 1) and the electron density lower limit value given by Eq. (3) is $1.86 \times 10^{16} \text{ cm}^{-3}$. The experimentally calculated electron density values (Table 3) are greater than this value, which is agreed with the assumption that the LTE predominates in the plasma.

IV. CONCLUSION

This paper encompasses the application of LIBS to soil analysis in the desert and the composed plasma characterization. More than hundreds of spectral lines are highly resolved for elemental composition of natural soil samples. The observed results indicated that electron temperature and density of the observed plasma depend on the sample matrix. These, consequently, alter the spectral characteristics of each element in the same soil matrix. The time resolved measurements of plasma parameters revealed that both T_e and N_e reach maximum values at 2.5 μs then slow recombination processes take place at later times. This plasma performance is contrasted with the fast plasma recombination of metallic materials found before. Furthermore, the LTE conditions are verified for the observed plasma measurements. This study is important for improving LIBS as a calibration-free technique in environmental applications. The later could be achieved in the future by measuring plasma parameters of only a single element as an indicator to recognize the desert soil matrix composition without analyzing that matrix and without ordinary calibration curves, thus saving a lot of time and effort.

ACKNOWLEDGMENT

This project was supported by King Saud University, Deanship of Scientific Research, College of Science Research Center.

REFERENCES

1. F. J. Fortes and J. J. Laserna, "The development of fieldable laser-induced breakdown spectrometer: No limits on the horizon," *Spectrochimica Acta Part B: Atomic Spectroscopy* **65**, 975-990 (2010).
2. J. J. Camacho, L. Díaz, M. Santos, L. J. Juan, and J. M. L. Poyato, "Time-resolved optical emission spectroscopy of laser-produced air plasma," *J. Appl. Phys.* **107**, 083306-1~083306-9 (2010).
3. W. A. Farooq, F. N. Al-Mutairi, and Z. A. Alahmed, "Analysis of rocks around capital of Kingdom of Saudi Arabia using laser induced breakdown spectroscopy," *Optics and Spectroscopy* **115**, 241-248 (2013).
4. J. I. Yun, "Material dependence of laser-induced breakdown of colloidal particles in water," *J. Opt. Soc. Korea* **11**, 34-39 (2007).
5. W. T. Y. Mohamed, "Fast LIBS identification of aluminum alloys," *Progress in Physics* **2**, 87-92 (2007).
6. R. M. da Silva, D. M. B. P. Milori, E. C. Ferreira, E. J. Ferreira, F. J. Krug, and L. Martin-Neto, "Total carbon measurement in whole tropical soil sample," *Spectrochimica Acta Part B: Atomic Spectroscopy* **63**, 1221-1224 (2008).
7. D. Santos Jr., L. C. Nunes, L. C. Trevizan, Q. Godoi, F. O. Leme, J. W. B. Braga, and F. J. Krug, "Evaluation of laser induced breakdown spectroscopy for cadmium determination in soils," *Spectrochimica Acta Part B: Atomic Spectroscopy* **64**, 1073-1078 (2009).
8. NIST Atomic Spectra Database, cited 2012 September 24, <http://www.nist.gov/atomic-spectroscopy.cfm>.
9. W. T. Y. Mohamed, "Fast LIBS identification of aluminum alloys," *Progress in Physics* **2**, 87-92 (2007).
10. H. R. Griem, *Plasma Spectroscopy* (McGraw-Hill, NY, USA, 1964), <http://griem.ospm.fr>.
11. M. A. Ismail, H. Imam, A. Elhassan, W. T. Youniss, and M. A. Harith, "LIBS limit of detection and plasma parameters of some elements in two different metallic matrices," *J. Anal. At. Spectrom.* **19**, 1-7 (2004).
12. W. T. Y. Mohamed, "Improved LIBS limit of detection of Be, Mg, Si, Mn, Fe and Cu in aluminum alloy sample using a portable Echelle spectrometer with ICCD camera," *Optics & Laser Technology* **40**, 30-38 (2008).
13. M. Sabsabi, V. Detalle, M. Harith, W. Tawfik, and H. Imam, "Comparative study of two new commercial echelle spectrometers equipped with intensified CCD for analysis of laser-induced breakdown spectroscopy," *Appl. Opt.* **42**, 6094-6098 (2003).
14. I. Zinovik and A. Povitsky, "Dynamics of multiple plumes in laser ablation: Modeling of the shielding effect," *J. Appl. Phys.* **100**, 024911 (2006).
15. K. M. Kim, J. H. Chung, and J. H. Ryu, "Thin film deposition of Tb₃Al₅O₁₂: Ce by pulsed laser ablation and effects of low-temperature post-annealing," *J. Opt. Soc. Korea* **16**, 76-79 (2012).
16. M. S. Dimitrijević, "Stark broadening of singly-ionized iron spectral lines," *Astron. Astrophys. Suppl. Series* **111**, 565-568 (1995).
17. R. W. P. McWhirter, *In Plasma Diagnostic Techniques*, R. H. Huddlestone and S. L. Leonard, eds (Academic Press, New York, USA, 1965), Chapter 5, p. 206.
18. G. Bekefi, *Principles of Laser Plasmas* (Wiley, New York, USA, 1976), pp. 550-605.